Biochimica et Biophysica Acta, 1015 (1990) 322–333
Elsevier

BBABIO 43126

Trapping kinetics, annihilation, and quantum yield in the photosynthetic purple bacterium *Rps. viridis* as revealed by electric measurement of the primary charge separation

H.-W. Trissl [1], J. Breton [2], J. Deprez [2], A. Dobek [2,3] and W. Leibl [1,*]

[1] *University of Osnabrück, Fachbereich Biologie / Chemie, Biophysik, Osnabrück (F.R.G.),*
[2] *Service de Biophysique, Département de Biologie, Centre d'Etudes Nucléaires de Saclay, Gif-Sur-Yvette (France)*
and [3] *Institute of Physics, A. Mickiewicz University, Poznan (Poland)*

(Received 23 May 1989)
(Revised manuscript received 19 September 1989)

Key words: Photovoltage; Photosynthesis; Quantum yield; Annihilation; Exciton trapping; Charge separation

The kinetics and the yield of the primary charge separation in whole cells of *Rps. viridis* was studied with the light-gradient technique using 30 ps and 12 ns flashes at 532 nm and 1064 nm. When the menaquinone acceptor, Q_A, of the reaction centers (RCs) is oxidized the primary charge separation occurs with two electrogenic phases. The faster phase with a time constant of 45 ± 20 ps contributed with 40% and the slower phase with a time constant of 140 ± 15 ps contributed with 60% to the total electrogenicity. We interpret the fast phase as the trapping time, monitored by the charge separation between the primary donor P-965 and the intermediary pheophytin acceptor, H. The second phase is ascribed to the electron transfer from H to Q_A. The reduction of Q_A, either chemically or photochemically, prior to the flash leaves only the fast rising phase. This signal decays with a time constant of 2.3–2.8 ns. At the excitation wavelength of 1064 nm the quantum yield of primary photochemistry is 0.97 ± 0.07. The reduction of Q_A does not change the quantum yield. The recombination of the state P^+H^- when Q_A is reduced can repopulate the excited state (ant.· P)* as demonstrated by a fluorescence phase with the same time constant. The fast phase of fluorescence was not affected by the reduction of Q_A, indicating an unaffected primary photochemistry. Fluorescence measurements with double flashes delayed by nanoseconds showed that the quenching power of P^+ is approx. 1.4-times smaller than that of P. A comparison of the photovoltage amplitude evoked by 12 ns flashes and 30 ps flashes at 1064 nm revealed marked competition between annihilation and trapping. At 532 nm the competition was less pronounced. The influence of the fraction of closed RCs (as defined by the state $P^+Q_A^-$) on the trapping efficiency was studied by excitation with trains of 30 ps flashes. These data and the data resulting from the nanosecond versus picosecond measurements are analyzed with a theory for the light-gradient photovoltage (Leibl and Trissl (1990) Biochim. Biophys. Acta 1015, 304–312) and a theory of exciton dynamics in the lake model (Deprez et al. (1990) Biochim. Biophys. Acta 1015, 295–303).

List of terms used

A_i	electrogenicity factors (dimensionless)	N	average size of a photosynthetic unit
α	coefficient relating the competition between annihilation and trapping	Δq_c	fraction of RCs closed by the flash
		Q_o	fraction of open RCs before the flash
E	energy of excitation flash (photons·cm^{-2} or μJ·cm^{-2})	q_{of}	fraction of open RCs after the flash
ε_i	dielectric constants	σ	absorption cross section of one mean antenna pigment
f	proportionality factor in the light-gradient theory	T_{eff}	transmission of one membrane of an effective vesicle
Γ	quantum yield of primary photosynthetic charge separation	τ_i	times constants
γ_i	bimolecular singlet-singlet annihilation rate constants	V	photovoltage
k_i	rate constants	V_o	photovoltage created by closure of all RCs
λ	wavelength	z, z_i	normalized excitation energies in hits per trap ($z = N \cdot \sigma \cdot E$)

Abbreviations: ant., antenna pigments; P-965, primary donor; H, intermediary pheophytin acceptor; Q_A, first quinonic acceptor; RC, reaction center; PSU, photosynthetic unit.

* Present address: CEN Saclay, France.
Correspondence: H.-W. Trissl, University of Osnabrück, F.B. Biologie/Chemie, Biophysik, Barbarastrasse 11, D-4500 Osnabrück, F.R.G.

Introduction

The first photophysical steps in bacterial photosynthesis are the absorption of light by a photochemically inactive antenna pigment, the migration of the excitation energy in the antenna bed, and its interaction with the primary donor, P, of the reaction center (RC) [1–3]. The redox potential of P* is sufficiently negative as to reduce an intermediary acceptor, H, which in turn reduces a quinonic acceptor, Q_A. In the case of *Rhodopseudomonas viridis* and *Rhodobacter sphaeroides*, the geometrical position of H, when projected onto the membrane normal, is close to the middle point between P and Q_A [4–6]. Since P and Q_A lie on opposite sides of the membrane the photochemical steps are electrogenic. Hence, the primary reactions can be divided into the non-electrogenic energy transfer and two electrogenic steps. The electrogenicity of the two forward electron transfer steps has been demonstrated by direct electrical measurements [7,8].

In the case of the purple bacteria *Rps. viridis* and *Rb. sphaeroides,* the protein structure of the RC, the pigment composition, and the spatial arrangement of the pigments are well known from X-ray crystallographic analysis [4–6]. Less detailed information exists on the dielectric properties of the micro-environment of the electron carrier molecules. As will be shown later, such information can be gained from an analysis of the electrical data in relation to the structure.

Also well known are the primary photophysical and photochemical reactions in isolated RCs of *Rps. viridis* down to femtosecond resolution. In RCs with oxidized Q_A the radical pair, P^+H^-, is formed with a rate constant of $(2.8\ ps)^{-1}$ [9]. Upon reduction of Q_A, the rate has been shown to be about 30–40% lower in *Rb. sphaeroides,* (Refs. 10, 11, and Martin, J.L. and Breton, J., unpublished results) and a value of $(6\ ps)^{-1}$ has been reported for *Rps. viridis* [12]. The reduction of Q_A has been reported to occur in about 230 ps [13].

A charge transfer state formed from P* in less than 200 fs has been proposed from hole-burning, photon-echo studies [14–16], as well as Stark effect spectroscopy [17]. The relevance of this step for the mechanism of trapping, however, is not completely clear.

In some purple bacteria, like *Rb. sphaeroides,* three different antenna pigment systems are distinguished [18]. These are the peripheral light-harvesting complex (LHC) B800-850, the core complex B875 [2,18], and some minor far-red absorbing pigments absorb around 900 nm [19,20]. Recent excitation transfer dynamic studies have shown that excitons created in the peripheral antenna flow energetically downhill via the core complex, to finally concentrate in far-red pigments that surround the RC [21]. As already recognized in 1965 by Holt and Clayton [22], the excitation of the primary donor, P-870, would require an energy uphill conversion. The corresponding Boltzmann factor of 0.2 at room temperature appears rather small in view of the short trapping time of about 60 ps [2,23].

A much higher energy gap is found in *Rps. viridis.* This bacterium contains only one antenna pigment system which – on the basis of its long-wavelength absorption maximum at 1015 nm – may be considered as a particularly far-red shifted core complex. The absorption maximum of the primary donor lies at 965 nm, thus at a much shorter wavelength than the antenna. This is the highest energy gap known so far and one would expect that – due to the very unfavorable Boltzmann factor – this may lead to a low photosynthetic quantum yield and to long trapping times. Low dose electron microscopy has shown that on the cytoplasmic side each RC is surrounded by 12 subunits which are assigned to antenna complexes [24,25]. Each subunit contains an α,β-polypeptide heterodimer, as well as a γ-polypeptide which does not bind bacteriochlorophyll [26]. If each of the α- and β-polypeptides binds one bacteriochlorophyll *b*, as it is generally accepted for bacteriochlorophyll-*a*-containing antenna [27], the antenna size is 24.

Rps. viridis is most interesting for studying exciton dynamics and trapping yield since the antenna system appears to be small and homogeneous and the RC structure and function are known in great details. On the other hand, little is known on the coupling of the antenna to the RC. This is in part due to technical problems associated with the classical assay of time resolved fluorescence in the near-infrared.

In contrast, photovoltage measurements can conveniently be applied to this organism. Recently, we have determined two rising phases in the primary charge separation by the light-gradient technique and have given a lower limit of 40 ps or less for the trapping time [8]. Technical improvements of the method [28] and newly developed theories of the light-gradient photovoltage [29], and exciton dynamics [30], led us to reinvestigate the primary photochemistry of this system in more detail.

The present study, carried out with whole *Rps. viridis* cells, aims at gaining information on (i) the absolute quantum yield of primary photochemistry upon excitation in the antennae, (ii) the trapping times in the low energy limit and at higher energies, (iii) the question whether a negative charge on Q_A, which is known to slow down the primary charge separation in isolated RCs, influences the trapping time, (iv) the effect of the photon energy (excitation wavelength) on the trapping process, (v) the competition between trapping and annihilation when short (30 ps) and intense picosecond flashes are applied, and (vi) the influence of the closure of a fraction of RCs (P^+) on the trapping efficiency of the remaining open RCs.

All these data were obtained from photovoltage mea-

surements of the light-gradient type. They were analysed with theories of the light-gradient [29] and of the exciton dynamics for the lake model description of photosynthetic units [30], which was shown to be adequate for *Rps. viridis* [31]. Further subjects addressed are: (i) the analysis of the photoelectric data for the dielectric position of H with respect to P and Q_A, (ii) the determination of the back-reaction kinetics under reducing conditions, and (iii) the measurement of the fluorescence yields and fluorescence decay kinetics (300 ps time resolution) under ambient and reducing conditions.

Materials and Methods

Rps. viridis cells were grown according to Ref. 32. For measurements, they were diluted with 20 mM Tris buffer (pH 8.0) to give an absorbance at 532 nm of $A = 0.34$ in a 0.1 mm cuvette. All measurements were done in the presence of 30 μM PMS (phenazine methosulfate).

Photoelectric measurements were carried out with a micro-coaxial cell as described [28]. The signals with the highest time resolution were amplified by two cascaded broad band amplifiers of 10 GHz and 8 GHz bandwidth (SHF 80 from SHF-Design, Berlin, and IV 74 from the Hahn-Meitner-Institut, Berlin). Single traces were recorded with a 7 GHz transient digitizing oscilloscope (7250, Tektronix). At the end of each sweep a marker signal from a picosecond photodiode was added, which had a fixed time delay to the excitation flash. The marker signal served to shift on a computer the individual traces to a common origin before averaging. This procedure avoids a loss of the time resolution due to the jitter between different single-shot traces. When lower time resolution was sufficient the signals were recorded with a 1 GHz set-up as described [28].

The time resolution and apparatus response function, including the laser flash duration, the response time of the micro-coaxial cell, of the two amplifiers, and of the oscilloscope, was obtained by means of the ultra-fast charge separation occurring in purple membranes [33,34]. Photovoltage signals of this system were found to display a Gaussian rise with a time constant of 85 ps. With the convolution procedure described in Ref. 23, this allows for the determination of exponential rise times of 20 to 40 ps depending on the signal-to-noise ratio.

Excitation pulses were derived from two different lasers. One was a Nd-YAG laser delivering flashes of 12 ns or 30 ps duration at the wavelengths of either 1064 nm or 532 nm (frequency doubled). The other was a ruby laser delivering flashes of 80 ns duration under Q-switched conditions or 30 ps duration under mode-locking conditions at the wavelength of 694 nm. For the fluorescence double-flash experiments (Fig. 7), the Q-switched ruby laser pulse was shortened to about 10 ns by means of a pulse clipping system. Double flashes spaced by 40 ns were obtained by means of a beam splitter and an optical delay line.

The flashes were passed through a light pipe to achieve homogeneous illumination. The distance between the measuring cell and the output of the light pipe was 70 mm, enlarging the homogeneously illuminated area to more than 10 mm diameter. Flash energies were measured with an energy meter (RJ 7200, Laser Precision) under the same geometry. The repetition rate was 0.1 Hz throughout.

Fluorescence was detected by a Ge-Avalanche picosecond photodiode (AR-G20, Antel) using a long-pass filter RG 835. The signals were amplified 10-times (B&H Electronics 3 GHz-amplifier, type AC-3010) and recorded on the 1 GHz set-up.

The absorption cross-section of the antenna pigments in the native membrane was determined as follows. An absorption spectrum of an aqueous suspension of *Rps. viridis* chromatophores was taken between 400 and 1100 nm on a Schimadzu spectrophotometer (model UV-160). 100 μl of the same suspension in 400 μl methanol was introduced on a filter (Sep-Pak C_{18} cartridge, Waters Associates, U.S.A.) and washed with 1 ml of 80% methanol/20% water. After turning the filter, bacteriochlorophyll *b* was extracted with 98% ethanol (2–3 ml). The first appearing BChl *b* was collected separately from the later appearing carotenoids. From the absorption of the BChl *b*-containing fractions and a molar absorption coefficient for the Q_y-band of bacteriochlorophyll *b* in ethanol of 77000 (Wollenweber, A., personal communication), we calculated the molar absorption coefficients of the membrane-bound antenna-BChl *b* to be 150000 at 1015 nm and 22500 at 1064 nm. The former is at variance with the absorption coefficients assumed by Olson and Nadler [35]. Applying the same procedure at 532 nm, yields an analytical molar extinction coefficient of 25300, which, however, involves a systematic underestimation due to the absorption of pigments other than BChl *b* in the membrane fraction (e.g., carotenoids and bacteriopheophytin).

Results

Excitation with 12 ns flashes

First we consider excitation conditions with long pulses for which annihilation effects can be neglected. These conditions allow the quantum yield of the primary photochemistry to be directly determined.

Excitation of whole *Rps. viridis* cells with 12-ns flashes of low energy ($< 100\ \mu J \cdot cm^{-2}$) at either 532 nm (Fig. 1a) or 1064 nm (Fig. 1b) led to a step function like photovoltage when the signals were measured with a high impedance amplifier (rise time 1 ns). Hence, the

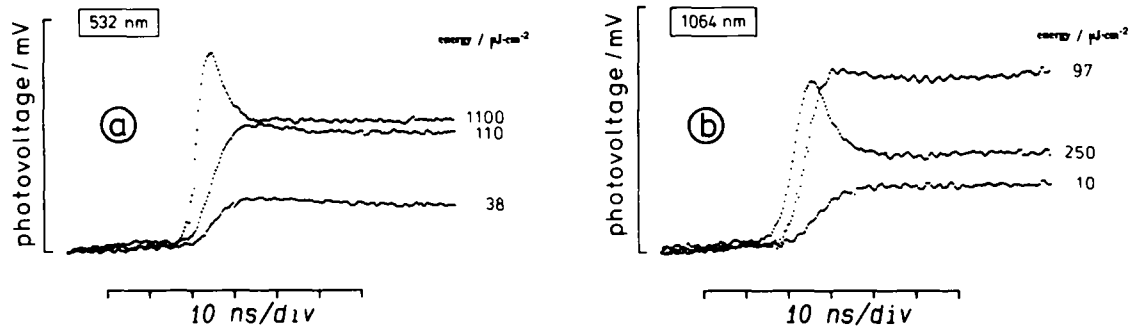

Fig. 1. Time resolved light-gradient photovoltages from *Rps. viridis* cells in a microcoaxial measuring cell excited with 12 ns laser flashes of different energies at the wavelengths 532 nm (a) and 1064 nm (b). The signals were picked up by a 500 MHz impedance converter (18 kΩ to 50 Ω) before their further amplification. Averaged traces: 20. The traces were deconvoluted with a 45 ns exponential decay function which results from a self-discharge of the capacitative measuring cell [50].

time-course of the small signals in Fig. 1 follows the integrated laser flash.

An increase of the flash energy above 100 $\mu J \cdot cm^{-2}$ led to a faster rising photovoltage, an increase of the maximal amplitude up to a saturation value, and a decrease of the photovoltage within the duration of the 12 ns flashes (Fig. 1a and b). These phenomena are specific for the light-gradient effect. They can be qualitatively understood and have been quantitatively treated (Eqn. 16 and Fig. 6 in Ref. 29).

The energy dependence of the photovoltage remaining after the 12 ns flash is plotted in Fig. 2 (double-logarithmic scales) for excitation at 532 nm (Fig. 2a) and 1064 nm (Fig. 2b), respectively. The data were analyzed using the correlation between the excitation energy expressed in hits per RC, z, and the fraction of still open RCs after a flash, q_{of}, in Eqn. 11 of the exciton theory for a lake model [30]. For the special case of negligible annihilation and of all RCs open before the flash ($Q_o = 1$) this equation reads:

$$\Gamma \cdot \frac{k_o}{k_c} \cdot z = q_{of} \cdot \left(1 - \frac{k_o}{k_c}\right) - \ln q_{of} + \left(\frac{k_o}{k_c} - 1\right) \quad (1)$$

The light-gradient photovoltage follows by substitution of Eqn. 1 into Eqn. 9 of the light-gradient theory [29]:

$$V(z) = f \cdot V_o \cdot [\Delta q_{c,1}(z) - \Delta q_{c,2}(T_{eff} \cdot z)] \quad (2)$$

using the relation $\Delta q_c = 1 - q_{of}$. Herein Γ means the quantum yield, k_o/k_c the ratio of quenching rate constants of open (P) and closed (P^+) RCs, V the measured photovoltage remaining after the flash, f a proportionality factor, V_o a hypothetical photovoltage which would be measured if all RCs in a single plane membrane were closed by the flash, and T_{eff} the transmission charac-

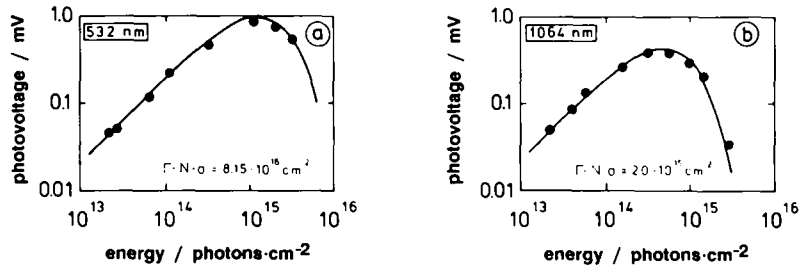

Fig. 2. Energy dependence of the photovoltage amplitudes remaining after the 12 ns flahses. (a) The data at 532 nm were fitted (solid line) as described in the text, using the following parameters: $f \cdot V_o = 12$ mV, $T_{eff} = 0.8$, $k_o/k_c = 1.4$, and $\Gamma \cdot N \cdot \sigma = 8.15 \cdot 10^{-16}$ cm^2. (b) The data at 1064 nm were fitted (solid line) using the following parameters: $f \cdot V_o = 12$ mV, $T_{eff} = 0.9$, $k_o/k_c = 1.4$, and $\Gamma \cdot N \cdot \sigma = 2.0 \cdot 10^{-15}$ cm^2.

TABLE I

List of parameters used in this work to fit all data

	T_{eff}	$\Gamma \cdot N \cdot \sigma$ (cm^2)	$f \cdot V_o$ (mV)	k_o/k_c	A_2/A_1	α
532 nm	0.8	$8.15 \cdot 10^{-16}$	12	1.4±0.2	1.5±0.05	1.2±0.1
1064 nm	0.9	$2.0 \cdot 10^{-15}$	12	1.4±0.2	1.5±0.05	2.6±0.2

terizing an 'effective' vesicle. The subscripts 1 and 2 refer to the upper and lower layer of the effective vesicle, respectively [29].

The ratio of the quenching rate constants of open and closed RCs was set to $k_o/k_c = 1.4$ as determined from fluorescence measurements (Fig. 7). The solutions of these equations were adjusted to the data with the parameters $f \cdot V_o$, T_{eff}, and $\Gamma \cdot N \cdot \sigma$ using the relation $z = N \cdot \sigma \cdot E$, where σ is the absorption cross section of a single antenna pigment and E the excitation energy. The parameters yielding the best fits (solid lines in Fig. 2) are listed in Table I.

Excitation with single 30 ps flashes

Next we consider excitation conditions with single 30 ps flashes and GHz-detection electronics which allows the electrogenic steps in the forward electron transfer, the trapping kinetics with open (PHQ_A) and reduced RCs (PHQ_A^-), the competition between trapping and

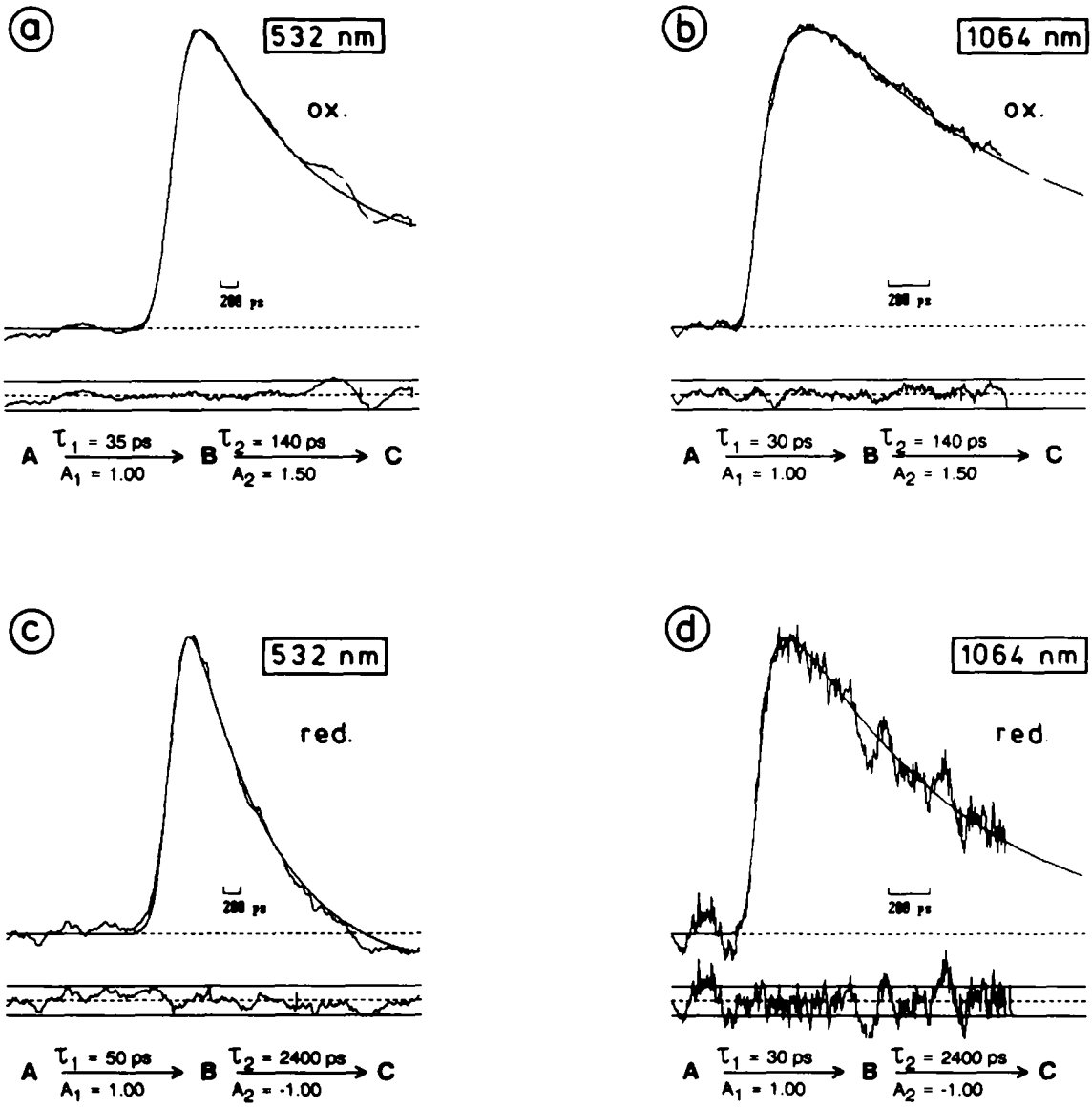

Fig. 3. Kinetics of the photovoltage from dark-adapted *Rps. viridis* cells with oxidized (a, b) and reduced (c, d) RCs elicited by 30 ps flashes. Reduction was achieved by a saturating preflash from a Q-switched ruby laser ($E = 2$–3 mJ·cm^{-2}), given 3–8 μs prior to the ps flash (c) or addition of 20 mM sodium dithionite (d). Excitation wavelengths: 532 nm (a, c); 1064 nm (b, d). Excitation energies: $E = 2.1 \cdot 10^{14}$ photons·cm^{-2} (a, c, d); $E = 2.7 \cdot 10^{14}$ photons·cm^{-2} (b). Number of averaged traces: 20 (a, b, d); 10 (c). Bandwidths: 1 GHz (a, c); 7 GHz (b, d). Impedances: 50 Ω (a–d). The traces below each photovoltage signal display the residuals between the measured traces and computer calculated curves according to a consecutive two-step electrogenic reaction convoluted with the response characteristics of the apparatus: Gaussian rise time of 88 ps, capacitative decay time of 0.90 ns, and an electrode polarization offset of 20% (determined by recordings on longer time scales). All amplitudes are normalized. The lines above and below the residuals mark the ±5% deviations.

annihilation, as well as the back-reaction kinetics when the RCs are reduced (PHQ_A^-) to be investigated.

The fast photovoltage from dark-adapted *Rps. viridis* cells evoked by 30 ps flashes of medium energy at 532 nm (1 GHz) and 1064 nm (7 GHz) is shown in Fig. 3a and b, respectively (note different time bases). The kinetics of the rising phase was fitted by an irreversible two-step reaction according to the scheme:

$$\text{ant.}^*\cdot P\cdot H\cdot Q_A \xrightarrow[A_1]{k_1} \text{ant.}\cdot P^+\cdot H^-\cdot Q_A \xrightarrow[A_2]{k_2} \text{ant.}\cdot P^+\cdot H\cdot Q_A^-$$

where 'ant.' stands for the antenna pigments, k_1 and k_2 are the rate constants, and A_1 and A_2 are the electrogenicity factors that describe the change of dipole strength belonging to each reaction step ($A_1 = 1.0$ by definition). In the above scheme, k_1 is the apparent rate constant for P^+H^- formation, which includes energy migration and charge separation. We define the reciprocal $(k_1)^{-1} = \tau_1$ as trapping time. The parameters that gave best fits to the traces are given below the figures. Fits of numerous traces obtained at various excitation energies gave $k_1 = (45 \pm 20\ \text{ps})^{-1}$, $k_2 = (140 \pm 15\ \text{ps})^{-1}$, and an electrogenicity ratio of $A_2/A_1 = 1.5$ at both wavelengths.

The reduction of the quinone, Q_A, by a saturating preflash or by dithionite caused a decrease of the photovoltage compared to that of the oxidized case, a cancellation of the slower 140 ps phase, and an acceleration of the decay. In Fig. 3c and d are shown the normalized photovoltages evoked by 30 ps flashes at 532 nm and 1064 nm, respectively. These and numerous other traces were analyzed according to the reaction scheme (neglecting a repopulation of the excited state):

$$\begin{array}{l}\text{ant.}^*\cdot P\cdot H\cdot Q_A^- \xrightarrow{k_1} \text{ant.}\cdot P^+\cdot H^-\cdot Q_A^- \\ \qquad\qquad\qquad\qquad \downarrow k_{-1} \\ \qquad\qquad\qquad\qquad \text{ant.}\cdot P\cdot H\cdot Q_A^-\end{array}$$

Due to the lack of the 140 ps phase, the analysis allowed a more precise determination of k_1 in the case of reduced RCs. Whereas the values found for k_1 in the dark-adapted case (PHQ_A) are so close to the time resolution of the present set-up, that they must be considered with precaution, the values $(55 \pm 20\ \text{ps})^{-1}$ found for k_1 in the reduced case (PHQ_A^-) at both 532 and 1064 nm can be considered to be time-resolved within the indicated error range.

The analysis for the rate constant of the back-reaction gave a value of $k_{-1} = (2.4\text{–}2.6\ \text{ns})^{-1}$, independent of the excitation energy at either wavelength. In isolated RCs with reduced Q_A, three fluorescence phases, of < 0.5, 2.5 and 15 ns, have been reported [36]. A 15 ns back-reaction in reduced RCs is also found by absorption spectroscopy [13]. Fits to the traces with two parallel phases for the back-reaction, 2.4–2.6 ns and 15 ns showed that under in vivo conditions a 2.4–2.6 ns back-reaction is the main decay route ($> 80\%$).

Comparison of the photovoltage amplitude of 12 ns and 30 ps excitation

The electrogenicity ratio A_2/A_1 can be obtained not only from the two phases of the forward charge separation, but also from the comparison of the photovolt-

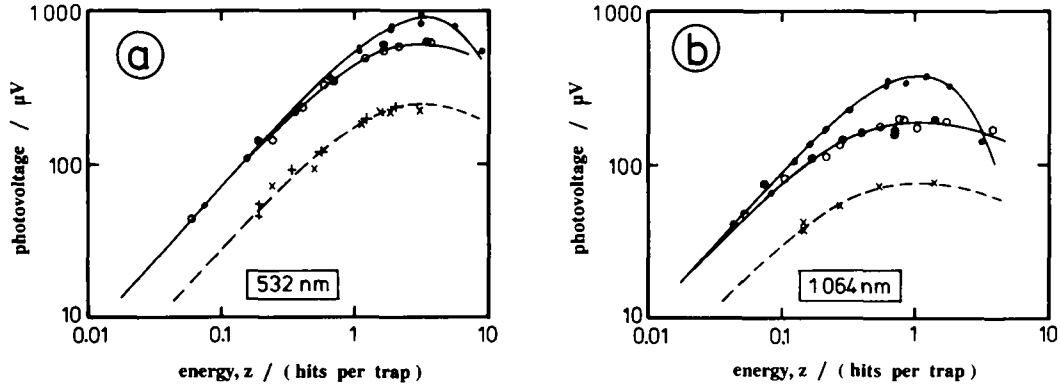

Fig. 4. (a) Comparison of the energy dependence of the photovoltage from *Rps. viridis* cells with oxidized Q_A (upper two curves) and reduced Q_A (lower curve) at the excitation wavelength of 532 nm. The uppermost curve contains data from 12 ns flashes (●) and the middle curve data from single 30 ps flashes (○), both recorded with high impedance at 1 GHz bandwidth. The middle curve also contains data from 30 ps flashes recorded with 50 Ω impedance at a bandwidth of either 1 or 7 GHz (⊗). The lower curve contains data from cells with reduced Q_A and 30 ps flashes recorded with 50 Ω impedance. Q_A was reduced either by 20 mM sodium dithionite and the photovoltage recorded at 7 GHz (+), or by a saturating preflash (3 mJ/cm²) from a Q-switched ruby laser applied 5 µs before the 30 ps flash and the photovoltage recorded at 1 GHz (×). The two upper curves were fit to the data by a simultaneous fit yielding the following set of parameters: light-gradient parameter $T_{eff} = 0.8$ and $f \cdot V_o = 12$ mV; annihilation parameter $\alpha = 1.2$, ratio of quenching rate constants $k_o/k_c = 1.4$. The lower dashed curve results from multiplication of the middle curve by 0.40. (b) Same as (a) but at the excitation wavelength of 1064 nm. The curve for reduced Q_A contains only data for which the reduction was achieved by a saturating preflash (3 mJ/cm²) from a Q-switched ruby laser 5 µs before the 30 ps flash, and the photovoltage was recorded at 1 GHz (×). The two upper curves were fit to the data by a simultaneous fit yielding the following set of parameters: light-gradient parameter $T_{eff} = 0.9$ and $f \cdot V_o = 12$ mV; annihilation parameter $\alpha = 2.8$ connectivity parameter $k_o/k_c = 1.4$. The lower fit curve (dashed) results from multiplication of the middle curve by 0.40. The energy scales are expressed as number of hits per trap, z, as described in the text.

age amplitudes under oxidizing and reducing conditions. These experiments require a time resolution of less than 1 ns because of the fast back-reaction of about 2.5 ns in the reduced case. They must therefore be carried out with picosecond flashes, where annihilation effects may play an important role.

The dependence of the peak photovoltage (measured with 1 GHz and 7 GHz electronics) on the excitation energy of 30 ps flashes at 532 nm and 1064 nm in the oxidized and reduced case is shown in Fig. 4a and b. For comparison, the photovoltage amplitudes evoked by Q-switched flashes (negligible annihilation) from Fig. 2 are included in Fig. 4. The energy scales were expressed in hits per RC, $z = N \cdot \sigma \cdot E$, taking the absorption cross-sections that follow from the molar absorption coefficients (see Materials and Methods) and $N = 24$. As σ at 532 nm is unknown, the z-scaling at this wavelength was done by assuming a quantum yield of $\Gamma = 0.35$ [35].

The picosecond data for the oxidized RCs in Fig. 4a and b were analyzed by substituting Eqn. 11 of Ref. 30 into Eqn. 2 for the special case in which all RCs are open before the flash ($Q_o = 1$):

$$(q_{of})^{\alpha} \cdot \left[\Gamma \cdot \frac{k_o}{k_c} \cdot z + \frac{k_o/k_c - 1}{\alpha - 1} + \frac{1}{\alpha} \right] = q_{of} \cdot \left(\frac{k_o/k_c - 1}{\alpha - 1} \right) + \frac{1}{\alpha} \quad (3)$$

The fit was made by taking the parameters already used before for the Q-switched data, and by introducing the annihilation parameter α as the only new adjustable parameter. The comparison of Q-switched and picosecond data under otherwise identical experimental conditions proves to be sensitive to the numerical value of α. This allows us to quote α with narrow limits: for 532 nm excitation $\alpha = 1.2$ and for 1064 nm excitation $\alpha = 2.6$ (see figure legend and Table I).

The picosecond data for reduced RCs in Fig. 4a and b were analyzed by the same set of parameters as used for the oxidized case, except that the amplitude was multiplied by a factor of 0.40 (dashed curves in Fig. 4 a and b). The error was estimated to be ± 0.015. Since the multiplication factor is connected to the electrogenicity factors by $A_1/(A_1 + A_2)$, it follows that $A_2/A_1 = 1.50 \pm 0.05$.

Excitation with trains of 30 ps flashes

Here we consider the effect of a variable fraction of closed RCs (P^+) on the trapping yield and on the competition between trapping and annihilation at 1064 nm where only the antenna pigments are excited. A progressive closure was achieved by successive flashes of the mode-locked Nd-YAG laser.

In Fig. 5a and b are shown the photovoltages evoked by a train of 30 ps flashes at low and high excitation energy, respectively. The photovoltage was measured with high impedance in order to allow the quantitative comparison with the Q-switched data. Analogous sets of data were also collected at 50 Ω impedance. They gave essentially the same results but with a better signal to noise ratio (data not shown; compare Ref. 28). The flashes are labeled by the integer, i, where $i = 0$ is given to the flash with the highest energy [28].

The amplitudes of the photovoltages, V_i, for the flash numbers, i, are replotted in Fig. 5c and d. Within the duration of the train, repopulation of P-965 can be neglected, due to the rereduction time of more than 230 ns [13,37]. Therefore, only the two states, PHQ_A and $P^+HQ_A^-$ are involved which allows the data to be analyzed by substituting Eqn. 11 of Ref. 30, which assumes the general case that a fraction of RCs (Q_o) is open before the flash:

$$\left(\frac{q_{of}}{Q_o} \right)^{\alpha} \cdot \left[\Gamma \cdot \frac{k_o}{k_c} \cdot z + Q_o \cdot \frac{k_o/k_c - 1}{\alpha - 1} + \frac{1}{\alpha} \right] = \frac{q_{of}}{Q_o} \cdot \frac{k_o/k_c - 1}{\alpha - 1} \cdot Q_o + \frac{1}{\alpha} \quad (4)$$

into Eqn. 14a of the light-gradient theory [29] in a successive manner:

$$V_i = f \cdot V_o \cdot [(Q_{o,1,i-1} - Q_{o,1,i}) - (Q_{o,2,i-1} - Q_{o,2,i})] \quad (5)$$

The fit was made by taking the parameters already used before (Table I) and no further adjustment parameter (Fig. 5c and d). This type of experiment is sensitive to the numerical values of α and k_c/k_o. The progressive closure of RCs as predicted by the theory is shown in Fig. 5e and f, using the parameters listed in Table I. These parameters consistently fit all our experimental data.

Fluorescence associated with PHQ_A/PHQ_A^-

To support by independent measurements the interpretation of the photoelectric data given before and the numerical values of the fit parameters, we measured the relative fluorescence yield and the fluorescence kinetics in the nano- and picosecond time range. These experiments were performed with a ruby laser ($\lambda = 694$ nm) instead of the frequency-doubled Nd-YAG laser in order to avoid distortions by the fundamental of the Nd-YAG at 1064 nm, a wavelength that lies within the fluorescence band of *Rps. viridis*.

Excitation of dark-adapted *Rps. viridis* cells with 80 ns flashes gave a fluorescence signal that followed strictly the time-course of the laser flash (Fig. 6a). Reduction of Q_A with dithionite caused the fluorescence to increase by a factor of about 1.4 (Fig. 6a). An increase by a factor of 1.6 has been reported in Ref. 38.

There are two possibilities to explain this fluorescence increase. The enhanced fluorescence may either originate from a longer lifetime of excitons in the antenna due to a slower trapping time, or from delayed fluorescence (i.e., luminescence) due to a charge recom-

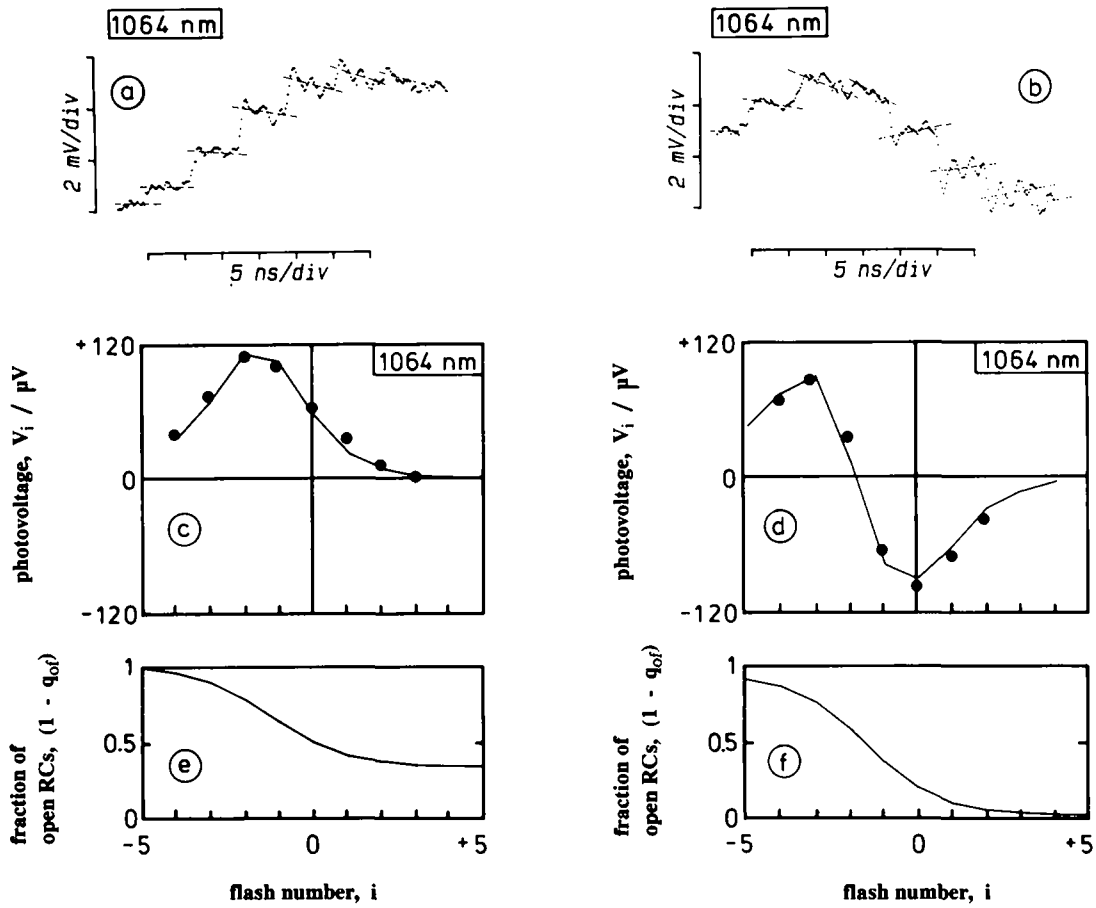

Fig. 5. Photovoltage from *Rps. viridis* cells excited with a train of 30 ps flashes (spaced by 6.8 ns) at a wavelength of 1.064 nm of a total energy of 115 $\mu J \cdot cm^{-2}$ (a) and 440 $\mu J \cdot cm^{-2}$ (b). The photovoltage was recorded with high impedance (see legend of Fig. 1) and on the 1 GHz set-up. The integrated energy was measured as described in Materials and Methods. The relative energy distribution to the flashes of the train was determined by a silicon PIN-diode which replaced the measuring cell. Averaged traces: 20. (c), (d) Comparison of the photovoltages with calculated amplitudes (straight lines) predicted by the light-gradient theory and by the exciton theory [29,30] taking the parameters listed in Table 1. (e), (f) Fraction of still open RCs after the ith flash. Further details of this type of experiment are found in Refs. [28,29].

bination between P^+H^- that repopulates the excited state. The first explanation would predict an increase of the yield of < 100 ps phases, the second the appearance of nanosecond phases.

When the fluorescence from dark-adapted *Rps. viridis* was measured with higher time resolution (1 GHz electronics) and non-saturating 30 ps excitation, a fast transient was found that decayed close to the base line within the photodiode's response time, about 200 ps (Fig. 6b; normalized amplitude). The reduction of Q_A by dithionite induced an additional slower decaying fluorescence phase with an exponential time constant in the range of 2.3–2.9 ns (Fig. 6c; normalized amplitude).

The fluorescence yield was obtained by deconvolution of the two phases. The ratio of the fluorescence yields for oxidized and reduced Q_A gave a ratio of 1.45, which is in good agreement with the measurement in Fig. 6a. The non-normalized data showed that the fast fluorescence transient had the same size and shape as in the oxidized case, except for the additional contribution of the slow phase (accuracy ± 10%).

This latter observation supplies indirect evidence that the trapping kinetics are not much affected by Q_A reduction. Furthermore, the 2.6 ns fluorescence phase correlates well with the electrically measured back-reaction, and can therefore be assigned to charge recombination luminescence.

Fluorescence associated with $PHQ_A / P^+HQ_A^-$

To analyze for a possible connectivity of photosynthetic units and to achieve a global analysis, it is essential to know the quenching efficiency of the state PHQ_A (or PHQ_A^-) and P^+HQ_A (or $P^+HQ_A^-$). Only when P^+ and P have different quenching efficiencies, will energy migration between neighbouring systems affect the overall trapping yield.

We determined the relative quenching power of P/P^+, i.e., k_o/k_c, by fluorescence measurements with double 10 ns flashes from a ruby laser. A first flash of variable energy served to close different fractions of RCs and a second weak probe flash served to measure the fluorescence yield (Fig. 7a).

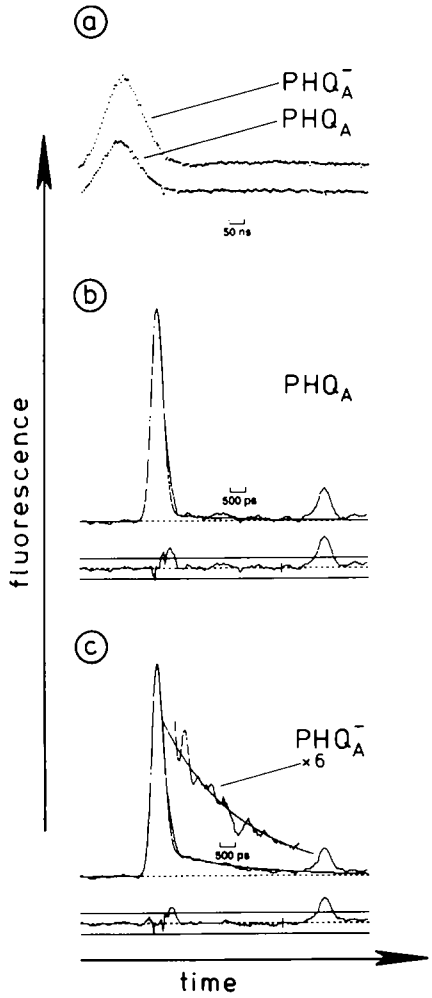

Fig. 6. (a) Fluorescence intensity evoked by 80 ns flashes at 694 nm from whole *Rps. viridis* cells with the RCs in the state PHQ_A (lower trace) and PHQ_A^- (upper trace). Averaged traces: 60. (b) Time-course of the fluorescence evoked by 30 ps flashes at 694 nm from *Rps. viridis* cells with open RCs. Averaged traces: 10. (c) Time-course of the fluorescence with reduced RCs. Averaged traces: 10. Inset: 6-times digitally amplified decaying phase together with a calculated fit with an exponential decay time constant of 2.4 ns. The second peak at the right end of the traces in b and c are due to reflections in the cable. Recording bandwidth: 1 GHz. Including the photodiode, the Gaussian time constant was 440 ps.

The dependence of the fluorescence yield of the probe flash on the energy of the first flash was measured at two energies of the probe flash. The amplitudes of the fluorescence of the probe flash are plotted in Fig. 7b as a function of the energy of the preflash. With increasing energy of the preflash the fluorescence yield increased by a factor of approx. 1.4. Under the assumption that the rate constant of trapping is much higher than the rate constant of losses in the antenna, this factor corresponds to the ratio k_o/k_c.

It should be noted that the extent of fluorescence increase upon oxidation of the primary donor is difficult to assess reliably by this experiment, since with increasing preflash energies the probability for triplet formation increases. The triplet states may form additional quenchers in addition to P^+ and obscure the pure effect of P/P^+ on the fluorescence yield. On the other hand, the situation in this double-flash experiment probably closely represents the true quenching states present in the photoelectric experiments.

Discussion

Quantum yields

The fit to the data in Fig. 2 yielded numerical values for the product $\Gamma \cdot N \cdot \sigma$ at the two excitation wavelengths. With knowledge of the corresponding absorption cross-sections of the antenna pigments and the antenna size of $N = 24$, the quantum yields would follow directly. However, at $\lambda = 532$ nm it is not possible to determine a meaningful absorption cross-section because of the difficulty to quantify at this wavelength the contributions of bacteriochlorophyll, bacteriopheophytin and carotenoids. Hence, we only can estimate from the fit parameter $\Gamma \cdot N \cdot \sigma$ a quantum yield at $\lambda = 532$ nm of about 0.35.

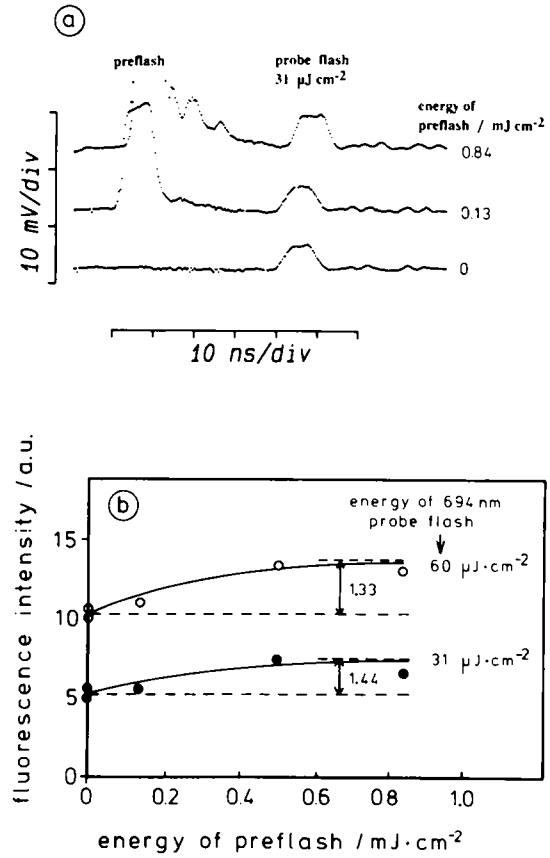

Fig. 7. (a) Time resolved fluorescence from dark-adapted whole *Rps. viridis* cells evoked by two 8 ns flashes at 694 nm. The preflash, probe flash, and fluorescence beams were all perpendicular to each other. The probe flash was derived from the preflash by means of a beam splitter and an optical delay line. The energies given in the figure refer to the front layer of the cuvette and represent an upper limit because of attenuation by absorption and light scattering. Averaged traces: 20. (b) Dependence of the fluorescence from the probe flash (two fixed energies) on the energy of the preflash.

At 1064 nm we determined the in vivo absorption cross-section to be $8.6 \cdot 10^{-17}$ cm^{-2} (see Materials and Methods). With this value, $N = 24$, and the experimental value $\Gamma \cdot N \cdot \sigma = 2.0 \cdot 10^{-15}$ cm^2 (Fig. 2), the quantum yield of primary charge separation is $\Gamma = 0.97$, a value most common in photosynthesis. We estimate the accuracy of this number to be within $\pm 7\%$.

The constant ratio of the photovoltage amplitudes under oxidizing and reducing conditions (Fig. 4) indicates that the term $\Gamma \cdot N \cdot \sigma$ in Eqn. 11a [30] must be the same in both cases. This means that the quantum yield Γ is unaffected by Q_A reduction, since neither N nor σ can be affected by the reduction of Q_A. Hence, the presence of a negative charge on Q_A does not much influence the P^+H^- formation, suggesting an irreversible trapping, i.e., a situation in which the equilibrium between the excited state in the antenna and P^+H^- rests largely on the charge separated state. This gives grounds for taking the same annihilation parameter α in the exciton theory for the oxidized and reduced case [30]. This finding is noticeably different from that of Photosystem II of green plants for which a strong influence of Q_A reduction on the P^+H^- yield is found [39,44].

Dielectric position of H

The dielectric position of H was determined in this study by several different experiments to be $A_2/A_1 = 1.5 \pm 0.05$. The value resulted firstly from the kinetic analysis of the two-step forward charge separation (1 and 7 GHz data, Fig. 3), and secondly from the comparison of the photovoltage amplitude with oxidized or reduced Q_A (Fig. 4). Data from experiments in which the reduction was achieved either by dithionite or a strong preflash were combined, the measuring conditions were varied from high to low impedance, and different set-ups were used (1 GHz and 7 GHz bandwidth). The finding of the same electrogenicity ratio from all the redundant experiments demonstrates the consistency of our analysis and the soundness of the number within the quoted error.

From the relative dielectric distances found by the photovoltage measurements and the known structural data of the *Rps. viridis* RC, it is possible to estimate the ratio of the dielectric constants of the environment of P-H and H-Q_A. This ratio is needed for the interpretation of electric field effects on the primary photochemistry [40]. Labeling the effective dielectric constant between P and H as ε_1 and that between H and Q_A as ε_2, and taking the corresponding geometric distances $(d_1/d_2) \approx 1$ [4,5], and our electrogenicity ratio of $(A_2/A_1) = 1.5$, $(\varepsilon_1/\varepsilon_2)$ can be calculated according to:

$$\varepsilon_1/\varepsilon_2 = \frac{A_2 \cdot d_1}{A_1 \cdot d_2} \approx 1.5 \qquad (6)$$

This means that the protein environment around P-H is more polar than around H-Q_A. This more polar surrounding might be essential for assisting the primary charge separation step [41,42].

Recently, the relative dielectric distance in PS II was reported to be $A_2/A_1 = 0.9 \pm 0.1$ [43,44]. If the geometric distances in the PS II reaction center are the same as in purple bacteria, as suggested by amino acid sequence homologies [45], then the ratio of the dielectric constants between P-H and H-Q_A in PS II is $\varepsilon_1/\varepsilon_2 = 1.1$. This significantly smaller ratio might be correlated with the slower electron transfer from H to Q_A: 140 ps in *Rps. viridis* (this work and Ref. 8) and 550 ps in PS II [39,43,44].

Trapping times with open and closed RCs

In photoelectric measurements the time needed to convert the excited state in the antenna system into the charge-separated state in the RC, i.e., the trapping time, is directly monitored. This assay has already been applied to *Rb. sphaeroides* R26.1 [23], and Photosystem I and Photosystem II of green plants [28,43,44]. In the low-energy limit the results were in agreement with fluorescence decay measurements.

In the present study the trapping time in *Rps. viridis* has been investigated at the two wavelengths, 532 and 1064 nm. The unknown transfer efficiency of the carotenoid, which makes the dominant contribution to the 532 nm absorption cross-section, prevents further interpretation of the data at this wavelength. At $\lambda = 1064$ nm, the energy dependence of the trapping time, τ_1, was estimated from a theory of exciton dynamics [30]. The fit to the experimental data yields in the low-energy limit trapping times of 45 ± 20 ps and 55 ± 20 ps for oxidized and reduced RCs, respectively. A lengthening of the trapping time could be expected if an equilibration of the excited state in the antenna system would exist which is depopulated with the rate constant of the primary charge separation, P^+H^-, and if the latter would decrease upon reduction of Q_A, as reported in Refs. 10, 11. The observation that, within our experimental error, the fast fluorescence phase is invariant upon reduction of Q_A (Fig. 6b, c) suggests the same trapping times for the two redox states of the quinone. This is also compatible with the photovoltage data.

The fast trapping time is consistent with the high quantum yield near 1 at 1064 nm, i.e., the fast depopulation of the excited state by the primary photochemistry before other decay paths become dominant. It is also consistent with the Förster rate constant calculated from the spectral overlap between the antenna fluorescence and the absorption of P (≈ 40 ps at a 20 Å distance and an orientation factor of 1.2; Trissl, unpublished calculations).

However, our model calculations based on (i) a thermal equilibration of the excitation energy over all an-

tenna pigments, (ii) a 2.8 ps primary charge separation, and (iii) accounting for the energy difference between antenna pigments and P by the Boltzmann factor, show that the observed trapping times are by a factor 5–10 faster than the theoretical predictions. For these calculations, the energy of the 0-0 transition of the primary donor was obtained from the absorption maximum and the 500 cm^{-1} Stokes' shift of P-965 [46], leading to a transition at 1014 nm. This value for the 0-0 transition of the primary donor agrees with recent low-temperature spectra [47] and hole-burning experiments [48]. A 240 cm^{-1} Stokes' shift for the antenna (1015 nm) in *Rps. viridis* can be deduced from the fluorescence spectrum [38]. The difference between the relaxed levels of P-965 and of the antenna is thus estimated to be 1.2 kT. Assuming total equilibration of the excitation energy, then the trapping time should not be faster than 120 ps.

The discrepancy could principally be ascribed to inappropriately estimated Stokes' shifts, although we consider this to be unlikely. Alternatively, the assumption of the 2.8 ps excited state depopulation step could also be wrong. Trapping times of about 40 ps could be modelled only with the assumption of a significantly faster relaxation process preceding the P^+H^- formation in 2.8 ps, which could be the formation of a charge transfer state as suggested by hole-burning and photon-echo studies [14,15]. A more detailed discussion on the consequences of our results for the trapping mechanism will be published elsewhere.

Competition between trapping and annihilation

The difference between the 12 ns data and the 30 ps data at 532 nm (Fig. 4a) and at 1064 nm (Fig. 4b) demonstrates significant losses of excitation energy with respect to the yield of $P^+HQ_A^-$ formation. In the exciton theory of Deprez et al. [30] this is accounted for by the annihilation parameter

$$\alpha = \frac{\gamma}{2 \cdot \Gamma \cdot k_o} \qquad (7)$$

where γ is an overall bimolecular decay rate constant of singlet-singlet annihilation [30,49]. With $\alpha = 2.6$ (Table I), $\Gamma = 1$, and $k_o = (45\ ps)^{-1}$ Eqn. 7 yields an annihilation rate constant of $\gamma = (8.6\ ps)^{-1}$ for 1064 nm excitation. For 532 nm excitation one calculates tentatively $\gamma = (54\ ps)^{-1}$ using $\alpha = 1.2$, $\Gamma = 0.35$, and $k_o = (45\ ps)^{-1}$. The large difference between the annihilation constants is tentatively related to the presence of a minor pool of carotenoids which significantly contributes to the absorption cross-section at 532 nm and which is different from the bulk antenna carotenoid pool absorbing at 480 nm (Breton, J., unpublished observation). Assuming that the minor population of carotenoids does not efficiently transfer energy to the RC, this would also explain the low quantum yield observed upon excitation at 532 nm. The competition between trapping and annihilation at 1064 nm in *Rps.viridis* ($\alpha = 2.6$) is in between the corresponding values found in *Rb. sphaeroides* R26.1 and *Rb. rubrum* [23,30].

Acknowledgements

The authors thank S. Andrianambinintsoa and Dr. G. Berger (CEN de Saclay) for their help in the BChl determination, Dr. W. Junge for helpful discussions and generous support of this work. The financial support of the Deutsche Forschungsgemeinschaft, Sonderforschungsbereich 171 is acknowledged.

References

1 Breton, J. and Geacintov, N.E. (1980) Biochim. Biophys. Acta 594, 1–32.
2 Van Grondelle, R. (1985) Biochim. Biophys. Acta 811, 147–195.
3 Geacintov, N.E. and Breton, J. (1987) C.R. Plant Sci. 5, 1–44.
4 Deisenhofer, J., Epp, O., Miki, K., Huber, R. and Michel, H. (1984) J. Mol. Biol. 180, 395–398.
5 Deisenhofer, J., Epp, O., Miki, K., Huber, R. and Michel, H. (1985) Nature 318, 618–624.
6 Allen, J.P., Feher, G., Yeates, T.O., Komiya, H. and Rees, D.C. (1987) Proc. Natl. Acad. Sci. USA 84, 5730–5734.
7 Trissl, H.-W. (1983) Proc. Natl. Acad. Sci. USA 80, 7173–7177.
8 Deprez, J., Trissl, H.-W. and Breton, J. (1986) Proc. Natl. Acad. Sci. USA 83, 1699–1703.
9 Breton, J., Martin, J.-L., Migus, A., Antonetti, A. and Orszag, A. (1986) Proc. Natl. Acad. Sci. USA 83, 5121–5125.
10 Woodbury, N.W., Becker, M., Middendorf, D. and Parson, W.W. (1985) Biochemistry 24, 7526–7531.
11 Breton, J., Martin, J.L., Migus, A., Antonetti, A. and Orszag, A. (1986) in Ultrafast Phenomena V (Fleming, G.R. and Siegman, A.E., eds.), pp. 393–397, Springer, Berlin.
12 Wasielewski, M.R. and Tiede, D.M. (1986) FEBS Lett. 204, 368–372.
13 Holten, D., Windsor, M.W., Parson, W.W. and Thornber, J.P. (1978) Biochim. Biphys Acta 501, 112–126.
14 Meech, S.R., Hoff, A.J. and Wiersma, D.A. (1985) Chem. Phys. Lett. 121, 287–292.
15 Boxer, S.G., Middendorf, T.R. and Lockhart, D.J. (1986) FEBS Lett. 200, 237–241.
16 Meech, S.R., Hoff, A.J., and Wiersma, D.A. (1986) Proc. Natl. Acad. Sci. USA 83, 9464–9468.
17 Lockhart, D.J. and Boxer, S.G. (1988) Proc. Natl. Acad. Sci. USA 85, 107–111.
18 Zuber, H. (1987) in The Light Reactions (Barber, J., ed.), pp. 197–259, Elsevier, Amsterdam.
19 Van Grondelle, R., Bergström, H., Sundström, V. and Gillbro, T. (1986) Biochim. Biophys. Acta 851, 431–446.
20 Van Grondelle, R., Bergström, H., Sundström, V., Van Dorssen, R.J., Voss, M. and Hunter, C.N. (1988) in Photosynthetic Light-Harvesting Systems (Scheer, H. and Schneider, S., eds.), pp. 519–530, Walter de Gruyter, Berlin.
21 Van Grondelle, R., Bergström, H., Sundström, V. and Gillbro, T. (1987) Biochim. Biophys. Acta 894, 313–326.
22 Holt, A.S. and Clayton, R.K. (1965) Photochem. Photobiol. 4, 829–831.
23 Dobek, A., Deprez, J., Paillotin, G., Leibl, W., Trissl, H.-W. and Breton, J. (1990) Biochim. Biophys. Acta 1015, 313–321.

24 Miller, K.R. (1982) Nature 300, 53–55.
25 Stark, W., Kühlbrandt, W., Wildhaber, I., Wehrli, E. and Mühlethaler, K. (1984) EMBO J. 3, 777–783.
26 Stark, W., Jay, F. and Mühlethaler, K. (1986) Arch. Microbiol. 146, 130–133.
27 Zuber, H. (1987) in Topics in Photosynthesis, Vol. 8 (Barber, J., ed.), pp. 197–259, Elsevier, Amsterdam.
28 Trissl, H.-W., Leibl, W., Deprez, J., Dobek, A. and Breton, J. (1987) Biochim. Biophys. Acta 893, 320–332.
29 Leibl, W. and Trissl, H.-W. (1990) Biochim. Biophys. Acta 1015, 304–312.
30 Deprez, J., Paillotin, G., Dobek, A., Leibl, W., Trissl, H.-W. and Breton, J. (1990) Biochim. Biophys. Acta 1015, 295–303.
31 Clayton, R.K. (1966) Photochem. Photobiol. 5, 807–821.
32 Cohen-Bazire, G., Sistrom, W.R. and Stanier, R.Y. (1957) J. Cell Comp. Physiol. 49, 25–68.
33 Groma, G., Szabo, J. and Varo, Gy. (1984) Nature 308, 557–558.
34 Trissl, H.-W., Gärtner, W. and Leibl, W. (1989) Chem. Phys. Lett., 158, 515–518.
35 Olson, J.M. and Nadler, K.D. (1965) Photochem. Photobiol. 4, 783–791.
36 Hörber, J.K.H., Göbel, W., Ogrodnik, A., Michel-Beyerle, M.E. and Cogdell, R.J. (1986) FEBS Lett. 198, 268–272.
37 Shopes, R.J., Levine, L.M.A., Holten, D. and Wraight, C.A. (1987) Photosynth. Res. 12, 165–180.
38 Carithers, R.P. and Parson, W.W. (1975) Biochim. Biophys. Acta 387, 194–211.
39 Schatz, G.H., Brock, H. and Holzwarth, A.R. (1988) Biopys. J. 54, 397–405.
40 Feher, G., Arno, T.R. and Okamura, M.Y. (1988) in The Photosynthetic Bacterial Reaction Center, pp. 271–287 (Breton, J. and Verméglio, A., eds.), pp. 271–287, NATO ASI Series, Vol. 149, Plenum, New York.
41 Creighton, S., Hwang, J.-K., Warshel, A., Parson, W.W. and Norris, J. (1988) Biochemistry 27, 774–781.
42 Michel-Beyerle, M.E., Plato, M., Deisenhofer, J., Michel, H., Bixon, M. and Jortner, J. (1988) Biochim. Biophys. Acta 932, 52–70.
43 Trissl, H.-W. and Leibl, W. (1989) FEBS Lett. 244, 85–88.
44 Leibl, W., Breton, J., Deprez, J. and Trissl, H.-W. (1989) Photosynth. Res. 22, 257–275.
45 Michel, H. and Deisenhofer, J. (1988) Biochemistry 27, 1–7.
46 Scherer, P.O.J., Fischer, S.F., Hörber, J.K.H. and Michel-Beyerle (1986) in Antennas and Reaction Centers of Photosynthetic Bacteria (Michel-Beyerle, M.E., ed.), pp. 131–137, Springer, Berlin.
47 Klevanik, A.V., Ganago, A.O., Shkuropatov, A.Ya. and Shuvalov, V.A. (1988) FEBS Lett. 237, 61–64.
48 Shuvalov, V.A., Klevanik, A.V., Ganago, A.O., Shkuropatov, A.Ya. and Gubanov, V.S. (1988) FEBS Lett. 237, 57–60.
49 Paillotin, G., Swenberg, C.E., Breton, J. and Geacintov, N.E. (1979) Biophys. J. 25, 513–534.
50 Trissl, H.-W. (1985) Biochim. Biophys. Acta 806, 124–135.